Journal of Solid State Chemistry 184 (2011) 3163–3171

Contents lists available at SciVerse ScienceDirect

Journal of Solid State Chemistry

journal homepage: www.elsevier.com/locate/jssc

X-ray absorption investigation of the valence state and electronic structure of $La_{1-x}Ca_xCoO_{3-\delta}$ in comparison with $La_{1-x}Sr_xCoO_{3-\delta}$ and $La_{1-x}Sr_xFeO_{3-\delta}$

O. Haas [a,*], Chr. Ludwig [b,c], U. Bergmann [d], R.N. Singh [e], A. Braun [f], T. Graule [f]

[a] Energy and Material Research Consulting, CH-6648 Minusio, Switzerland
[b] General Energy Research, Paul Scherrer Institut, CH-5232 Villigen PSI, Switzerland
[c] École Polytechnique Fédérale de Lausanne, ENAC-IIE, CH-1015 Lausanne, Switzerland
[d] Linac Coherent Light Source, SLAC National Accelerator Laboratory, Menlo Park, CA 94025, USA
[e] Banaras Hindu University, Chemistry Department, Varanasi 221005, India
[f] Empa, Swiss Federal Laboratories for Materials Science and Technology, Laboratory for High Performance Ceramics, CH-8600 Duebendorf, Switzerland

ARTICLE INFO

Article history:
Received 21 April 2011
Received in revised form
11 August 2011
Accepted 22 September 2011
Available online 29 September 2011

Keywords:
$La_{1-x}Ca_xCoO_{3-\delta}$
$La_{1-x}Sr_xCoO_{3-\delta}$
$La_{1-x}Sr_xFeO_{3-\delta}$ perovskites
X-ray absorption spectroscopy
Valence state
Electronic structure

ABSTRACT

3*d* metal K-shell X-ray absorption spectra of perovskites with the composition $La_{1-x}Ca_xCoO_{3-\delta}$ (x=0, 0.2, 0.4, 0.5, 0.6, 0.8), $La_{1-x}Sr_xCoO_{3-\delta}$ (x=0, 0.1, 0.2, 0.3, 0.4, 0.5) and $La_{1-x}Sr_xFeO_{3-\delta}$ (x=0, 0.2, 0.4, 0.5, 0.6, 0.8) are compared on the basis of pre-edges, white line features and extended fine structures. The measurements were performed at 300 K and for $La_{1-x}Ca_xCoO_{3-\delta}$ also at temperatures as low as 10–20 K. Going to low-temperature the measurements indicate an increase in t_{2g}^* and a decrease in e_g^* orbital occupancy, which is most accentuated in the $LaCoO_3$ sample. Virtually no Co K-edge shift was observed for the $La_{1-x}Ca_xCoO_{3-\delta}$ and $La_{1-x}Sr_xCoO_{3-\delta}$ compounds and the Co–O distances are also not significantly reduced when La^{3+} is partially substituted by Ca^{2+} or Sr^{2+}. From the pre-edge features of these perovskites we are tended to conclude that the t_{2g}^* orbitals are less, and the e_g^* orbitals are more occupied with increasing x in the Ca and Sr substituted compounds, whereas the total *d*-electron density is not changing. These results indicate that cobalt prefers a valence state of 3^+ in these Co perovskites. This could also be confirmed with iodometric titrations. The Fe perovskites behave differently. In contrast to the Co perovskites, for $La_{1-x}Sr_xFeO_{3-\delta}$ perovskites the Fe K-edge is shifted, the pre-edge features intensity is increasing and the Fe–O bond length is decreasing with increasing x. The valence states of the iron in the $La_{1-x}Sr_xFeO_{3-\delta}$ perovskites in fact increase as much as x increases.

1. Introduction

$La_{1-x}Ca_xCoO_{3-\delta}$, $La_{1-x}Sr_xCoO_{3-\delta}$ and $La_{1-x}Sr_xFeO_{3-\delta}$ perovskites have attractive electronic and ion-conduction properties, which offer applications in numerous domains. They are used as a catalyst in redox processes. $LaCoO_3$ for instance exhibits catalytic activity above 1000 K, where carbon monoxide can be oxidized and NO_x can be decomposed [1]. $La_{1-x}Ca_xCoO_{3-\delta}$ and $La_{1-x}Sr_xCoO_{3-\delta}$ can be used in oxygen diffusion electrodes as a catalyst to reduce and to evolve oxygen [2–4]. The oxygen-ion-conducting and electron-conducting properties of such perovskites can be used in high temperature fuel cell cathodes [5–8]. They show also promises for thermoelectric devices [9] and have interesting magnetic properties, e.g. high magneto-resistance or even negative magneto-resistance [10]. Magnetic anomalies and its temperature dependency [11–13] are another area of interest of these perovskites.

X-ray absorption spectroscopy (XAS) is a very valuable tool to study electronic and structural properties of materials. XAS has been developed over several decades, and standardized methods for data analysis are now available for near edge absorption (XANES), the extended X-ray absorption fine structure region (EXAFS) and its surface version (SEXAFS). Synchrotron radiation has extended the possibilities of these methods, since much higher X-ray intensities are available allowing faster measurements and the detection of lower concentrations. In many cases XAS, particularly based on hard X-rays with a large attenuation depth, can be used as an *in-situ* analytical tool [14] and has therefore tremendous advantages over most high-vacuum analytical methods. We used XAS to study the valence state and to obtain information about the electronic configuration of these Co and Fe perovskites. The valence states govern most of the physico-chemical properties of these perovskites. The valence state of the transition metal cation can be manipulated by partial substitution of La^{3+} using divalent earth metal ions like Ca^{2+} or Sr^{2+}. Especially the valence state of iron in such perovskites is substantially influenced by substitution of La with Ca^{2+} or Sr^{2+}.

* Corresponding author.
E-mail address: otto.haas@bluewin.ch (O. Haas).

0022-4596/$ - see front matter © 2011 Elsevier Inc. All rights reserved.
doi:10.1016/j.jssc.2011.09.027

Electrochemical methods can also be used to change the valence state [15]. The valence state may also depend on the oxidizing or reducing conditions during preparation [16]. The citric acid precursor method in example may lead to reduced perovskites since the citric acid is carbonized when the sample is fired and at high temperature this carbon may act as a reducing agent and influence the valence state. This is not the case if oxides are used as starting materials, but if they are heated too high, deoxygenation may also take place [17].

There are several publications about XAS investigations on $La_{1-x}Ca_xCoO_{3-\delta}$ [18–24], whereas to our knowledge low-temperature XAS studies were only performed on $LaCoO_3$ [18,20] and on $La_{1-x}Sr_xCoO_{3-\delta}$ [18,25]. XAS investigations on $La_{1-x}Sr_xFeO_{3-\delta}$ [26–29] and $La_{1-x}Sr_xCoO_{3-\delta}$ [30–35] should also be mentioned. In our former publications about $La_{1-x}Ca_xCoO_{3-\delta}$ [22] and $La_{1-x}Sr_xFeO_{3-\delta}$ [26] we discussed our XAS data together with the existing literature of these perovskites. In addition to these measurements we investigated now the $La_{1-x}Ca_xCoO_{3-\delta}$ series at low temperature (10–20 K) together with $La_{1-x}Sr_xCoO_{3-\delta}$ samples obtained from Prof. Singh. We think it is of general interest to compare the $La_{1-x}Sr_xCoO_{3-\delta}$ series and the cold measurements of the $La_{1-x}Ca_xCoO_{3-\delta}$ series with the former results obtained from $La_{1-x}Ca_xCoO_{3-\delta}$ and $La_{1-x}Sr_xFeO_{3-\delta}$ series presented in [22,26]. Concerning our new $La_{1-x}Sr_xCoO_{3-\delta}$ measurements we like to compare our work with the existing literature as follows:

Jiang et al. [25] investigated $La_{1-x}Sr_xCoO_{3-\delta}$ in a somewhat lower x range than we did but at room temperature and low temperature. They concentrated on a discussion about the Jahn–Teller effect in these perovskites and discussed the possibility of a core-hole potential interaction on the Co K-edge energy. It should be mentioned that their nanoparticle samples do not show the same x dependency of the Co K pre-edge as we present here. Toluemonde et al.'s work [18] is probably closest to our investigation and argumentation of the $La_{1-x}Sr_xCoO_{3-\delta}$ series but, they concentrated more on the O K edge and made no EXAFS investigation. In contradiction to Jiang et al. and our investigation, Toluemonde et al. suggested a mixed (LS–IS Co^{3+}/IS Co^{4+}) cobalt configuration. Hueso et al. [33] describe the influence of calcination to the crystal structure and electronic structure of $LaCoO_3$ and $La_{0.5}Sr_{0.5}CoO_{2.75}$. They confirmed our result obtained from the Co K pre-edge features with their O K-edge XAS spectra but have no Co K pre-edge discussion in their paper. They, however, introduced an interesting argument why Sr substitution of La would lead to a low field high spin configuration. None of the mentioned publications made a comparison of $La_{1-x}Sr_xCoO_{3-\delta}$ with $La_{1-x}Sr_xFeO_{3-\delta}$ and $La_{1-x}Ca_xCoO_{3-\delta}$. Piovano et al. [34] describe the electrochemical intercalation of oxygen ions in Brownmillerite phase $SrMO_{2.5}$. These experiments cannot be compared with our perovskites, where lanthanum is partially substituted by Sr. In fact their Co and Fe K pre-edge features behave completely different. The main focus of the present publication is the determination of the valence states of Co and Fe in the investigated perovskites with X-ray absorption spectroscopy. But we also discuss the influence of temperature and lanthanum substitution by Ca or Sr on the electronic structure and valence state of these perovskites.

2. Materials and methods

2.1. Synthesis of perovskites

$LaCoO_3$ and $La_{1-x}Ca_xCoO_{3-\delta}$ perovskites were prepared using the citrate acid precursor method [2]. Stoichiometric amounts of $La(NO_3)_3 \cdot 6H_2O$ (Fluka) and $Co(NO_3)_2 \cdot 6H_2O$ (Fluka) were added to an aqueous 1 M citric acid solution. The solution was evaporated at 343 K using a rotary evaporator and dried for 3 days at 363 K. The resulting powder was first heated in air at 473 K for 2 h and then calcined in air for another 2 h at 973–1023 K.

$La_{1-x}Sr_xCoO_{3-\delta}$ perovskites were obtained by the malic acid precursor route as reported in the literature [36].

$La_{1-x}Sr_xFeO_{3-\delta}$ perovskites (LSF) were prepared using $La(OH)_3$ (Auer Remy, 99.99%), $SrCO_3$ (Fluka, 98%) and Fe_2O_3 (Fluka, 99%) in stoichiometric quantities corresponding to the desired LSF composition. The powder was homogenized during 15 h in the ball mill with 5 mm ZrO_2 balls using 40 wt% of distilled water and 2 wt% of Dolapix CE 64 (Zschimmer&Schwarz, Germany) as liquefier. Subsequently the slurry was dried in a rotary evaporator (Büchi type R-134). The annealing was performed in Al_2O_3 crucibles in a muffle furnace (Ceram-Aix FHT 175/30) using a heating rate of 300 K/h up to the annealing temperature, which was held for 4 h and then cooled down with a cooling rate of 300 K/h. The slow cooling rate allowed the sample to heal oxygen vacancies, introduced at high annealing temperatures. The annealing temperature was adjusted for different *A*-site compositions until phase purity was achieved. For the desired *A*-site variation of the $La_{1-x}Sr_xFeO_{3-\delta}$ perovskites, 1573 K was found to be the optimal annealing temperature for all *A*-site variations. The phase composition was determined by powder XRD analysis (PANalytical X'Pert PRO, Cu-$K\alpha$). After annealing, the powders were milled down to the desired particle size < 1 μm by wet-ball milling. The slurry was finally dried with a rotary evaporator.

2.2. Iodometric titration

The perovskites were dissolved in 4 M HCl and titrated during dissolution. The titration was performed under rigorous oxygen exclusion using a 0.05 M $Na_2S_2O_3$ aqueous solution. The sample weight was corrected for water and CO_2 adsorption using thermogravimetry to evaluate the water and CO_2 contents. The procedure and the used apparatus have been described in a former publication [37].

2.3. X-ray absorption measurements

The powder samples of the perovskites were mixed with BN in a 1:5 ratio, and pressed to pellets for the X-ray absorption measurements. The Co amount per cm^2 in the pellet was adjusted to reach one absorption length using the X-ray absorption program offered by Lawrence Berkeley National Laboratory [38]. X-ray absorption measurements were carried out at beamline 9-3 at the Stanford Synchrotron Radiation Lightsource (SSRL), with the storage ring operating at 3 GeV beam energy and a beam current of 100 mA at the top of the fill. A Si(220) double-crystal monochromator was used for energy selection. The intensities of the incident and transmitted X-rays were monitored by nitrogen filled ionization chambers. The monochromator was scanned in energy from 200 eV below to 800 eV above the Co or Fe K absorption edge. The Co K edge X-ray absorption spectra of the $La_{1-x}Ca_xCoO_{3-\delta}$ perovskites were measured at 300 K and at about 10–20 K. A 7 μm thin Co or Fe foil was used as a reference. The foil and the $I_{reference}$ detector were positioned behind the sample along the direction: {X-ray beam/I_o – detector/[sample]/I_{sample} – detector/[metal foil]/$I_{reference}$ – detector}.

2.4. XAS data analysis

Reduction of the absorption data was performed with the software program WINXAS [39] using standard procedures. The resulting normalized $\chi(k)$ function was then transformed in the k-space and weighted with k^3 to account for dampening of oscillations with increasing k. The $k^3\chi(k)$ function was then

Fourier transformed in a limited k-range (1.5–15.0). A window based on Bessel functions with a beta parameter of 4 was used to diminish artifacts inferred by the finite Fourier filtering. The WINXAS program package was also used for the fitting of the $k^3\chi(k)$ function with theoretical scattering paths, which were generated with the FEFF8.20 program [40] using published atomic positions [41–43,22] of $LaCoO_3$ perovskite.

To generate the FEFF input files we used the atomic positions reported by Wold and Ward [41] for the cubic space group. We analyzed only the metal oxygen scattering part of the EXAFS spectrum. In these perovskites the oxygen is in most cases regularly octahedrally coordinated. The least square fit was performed with the multiple parameter optimization program provided by the WINXAS program package, which allows to extract the effective interatomic distance r_{eff} in Å as well as N: coordination number, ΔE_0: zero energy shift, σ^2: Debye–Waller factor, and S_0^2: amplitude reduction factor.

3. Results and discussion

3.1. Structure of the perovskites

In two previous publications the crystallographic structure of our samples as obtained by XRD was discussed in more detail [19,26]. Confirmation of the perovskite structure by XRD is essential with respect to the following EXAFS investigation. We may recall a number of important crystallographic details here for the reader because these are relevant for the later interpretation of the EXAFS data.

The structure of $LaCoO_3$ and $La_{1-x}Ca_xCoO_{3-\delta}$ has been investigated by different groups [37,38,44–47]. Initial inspection of the diffractograms suggests that $LaCoO_3$ and $La_{1-x}Ca_xCoO_{3-\delta}$ are cubic. Detailed XRD analysis however shows that the materials have slightly distorted angles so that the actual phase is therefore more accurately represented with the rhombohedral space group symmetry or even with the monoclinic $I2/a$ (ITC index #15) [43].

The XRD patterns of our samples correspond to the published data. (See spectra in supplemental material.) In a previous publication we discussed the influence of partial substitution of La by Ca [19]. The XRD's of the samples with Ca show somehow larger lines and more noise than the $LaCoO_3$ samples, which is expected due to the partial Ca^{2+} substitution of La^{3+} and the introduced random distributed oxygen vacancies or ligand holes. In addition, our Ca containing samples had rather high surface areas of about 15–20 m^2/g. Thermogravimetric measurements revealed small amounts of surface adsorbed CO_2, which leads to a small Bragg reflection at $2\theta = 29.4^\circ$ typical for $CaCO_3$. Storing the $La_{1-x}Ca_xCoO_{3-\delta}$ perovskites in air provokes slow erosion reaction with $CaCO_3$ production especially on samples with a high surface area.

The crystal structure investigation of $La_{1-x}Sr_xCoO_{3-\delta}$ (x= 0–0.5) by Efimov et al. [31] revealed rhombohedral $R-3c$ symmetry for the investigated x range. The XRD data of $La_{1-x}Sr_xCoO_{3-\delta}$ published by Singh et al. [4] (see spectra in supplemental material) indicated two phases at higher x values, which explains our FT $k^3\chi(k)$ function obtained from this sample.

3.1.1. XRD investigation $La_{1-x}Sr_xFeO_{3-\delta}$ series

In a former publication we reported on the structure of the $La_{1-x}Sr_xFeO_{3-\delta}$ samples [26] (see spectra in supplemental material) and found it in accordance with the literature [48] and in contradiction to $La_{1-x}Ca_xCoO_{3-\delta}$ and $La_{1-x}Sr_xCoO_{3-\delta}$ that d_{Fe-O} depends clearly on x. There are also more important structural changes. $LaFeO_3$ is orthorhombic ($Pbnm$, space group no. 62). Substitution of La by Sr increases the symmetry of the crystal structure, thus $La_{0.5}Sr_{0.5}FeO_{3-\delta}$ has a rhombohedral structure ($R-3c$, space group no. 167), and $SrFeO_{3-\delta}$ has a cubic symmetry ($Pm3m$, space group no. 221). In our former publication [26] we evaluated the following Fe–O distances: $LaFeO_3$, $d_{Fe-O1}=2.0087$ Å, $d_{Fe-O2}=2.0090$, $d_{Fe-O3}=2.0021$ Å, for $La_{0.5}Sr_{0.5}FeO_{3-\delta}$, $d_{Fe-O}=1.954$ Å and for $SrFeO_{3-\delta}$, $d_{Fe-O}=1.928$ Å. Compared to the d_{Co-O} values in $La_{1-x}Ca_xCoO_{3-\delta}$ perovskites the Fe–O distances are larger and depend strongly on x indicating a substantial increase in valence state with x. In fact the d_{Fe-O} distances of $LaFeO_3$ are typical for Fe (III) compounds, whereas the Fe–O distances of $SrFeO_{3-\delta}$ correspond well with Fe(IV) compounds.

3.2. Results XAS investigation

3.2.1. $La_{1-x}Ca_xCoO_{3-\delta}$ perovskites

For the present investigation we measured $La_{1-x}Ca_xCoO_{3-\delta}$ samples at 300 K and at 10–21 K. To our knowledge low temperature XAS data of $La_{1-x}Ca_xCoO_{3-\delta}$ samples have only been published from $LaCoO_3$ and not from Ca substituted samples. The first column of Fig. 1 shows the pre-edge region of the investigated $La_{1-x}Ca_xCoO_{3-\delta}$ samples. The second column shows the XANES regions (Co K-edge region), and the third column the Fourier transformed χ^*k^3 functions of the indicated samples. The 300 K and the low temperature spectra are presented in the same plots in Fig. 1, where the temperatures of the cold measurements are indicated in Kelvin. The pre-edge features (first column) reveal a t_{2g}–e_g multiplet structure with a redistribution of spectral weight during temperature change and also during change of the substitution parameter x with somewhat higher intensities at higher energies for the low temperature samples, which is especially the case for the $LaCoO_3$ sample. The main intensity of this multiplet shifts to lower energies with increasing x. The total intensities of the pre-edge features, however, remain constant with x for the $La_{1-x}Ca_xCoO_{3-\delta}$ series of Figs. 1 and 2. At the K-edge (second column) there are virtually no differences between the 300 K and low temperature spectra. This is also the case for the x dependency, where only the maximum of the edge is shifting somewhat but not the edge at half-height. The Fourier transformed $k^3\chi(k)$ functions shown in the third column of Figs. 1 and 2 reveal a strong intensity increase for the $k^3\chi(k)$ functions of the low temperature samples and an intensity decrease with increasing x. The FT $k^3\chi(k)$ function also exhibits a strong decrease with x at its second peak.

3.2.2. $La_{1-x}Sr_xCoO_{3-\delta}$ perovskites

In Fig. 2 the x-dependencies of $La_{1-x}Ca_xCoO_{3-\delta}$, $La_{1-x}Sr_xCoO_{3-\delta}$ and $La_{1-x}Sr_xFeO_{3-\delta}$ series are resumed with three representative x-values as indicated in the insets. The third row of Fig. 2 summarizes the XAS data of the $La_{1-x}Sr_xCoO_{3-\delta}$ series. The substitutional range for x=0–0.5 shows similar trends. In contrast to the $La_{1-x}Ca_xCoO_{3-\delta}$ series the total intensity of the pre-edge decreases slightly with increasing x.

3.2.3. $La_{1-x}Sr_xFeO_{3-\delta}$ perovskites

The fourth column of Fig. 2 shows the data of $La_{1-x}Sr_xFeO_{3-\delta}$ perovskites. In contrast to $La_{1-x}Ca_xCoO_{3-\delta}$ and $La_{1-x}Sr_xCoO_{3-\delta}$ where the total pre-edge feature intensity was constant or slightly decreasing with x the $La_{1-x}Sr_xFeO_{3-\delta}$ series exhibits a strong increase of the pre-edge multiplet with increasing x. It shows also a Fe K-edge shift with increasing x.

3.3. Discussion of the XAS results

3.3.1. Pre-edge of the $La_{1-x}Ca_xCoO_{3-\delta}$ and $La_{1-x}Sr_xCoO_{3-\delta}$ and $La_{1-x}Sr_xFeO_{3-\delta}$ series

The pre-edge features shown in the first column of Figs. 1 and 2 are due to quadrupolar $1s\rightarrow 3d$ transitions. These $1s\rightarrow 3d$

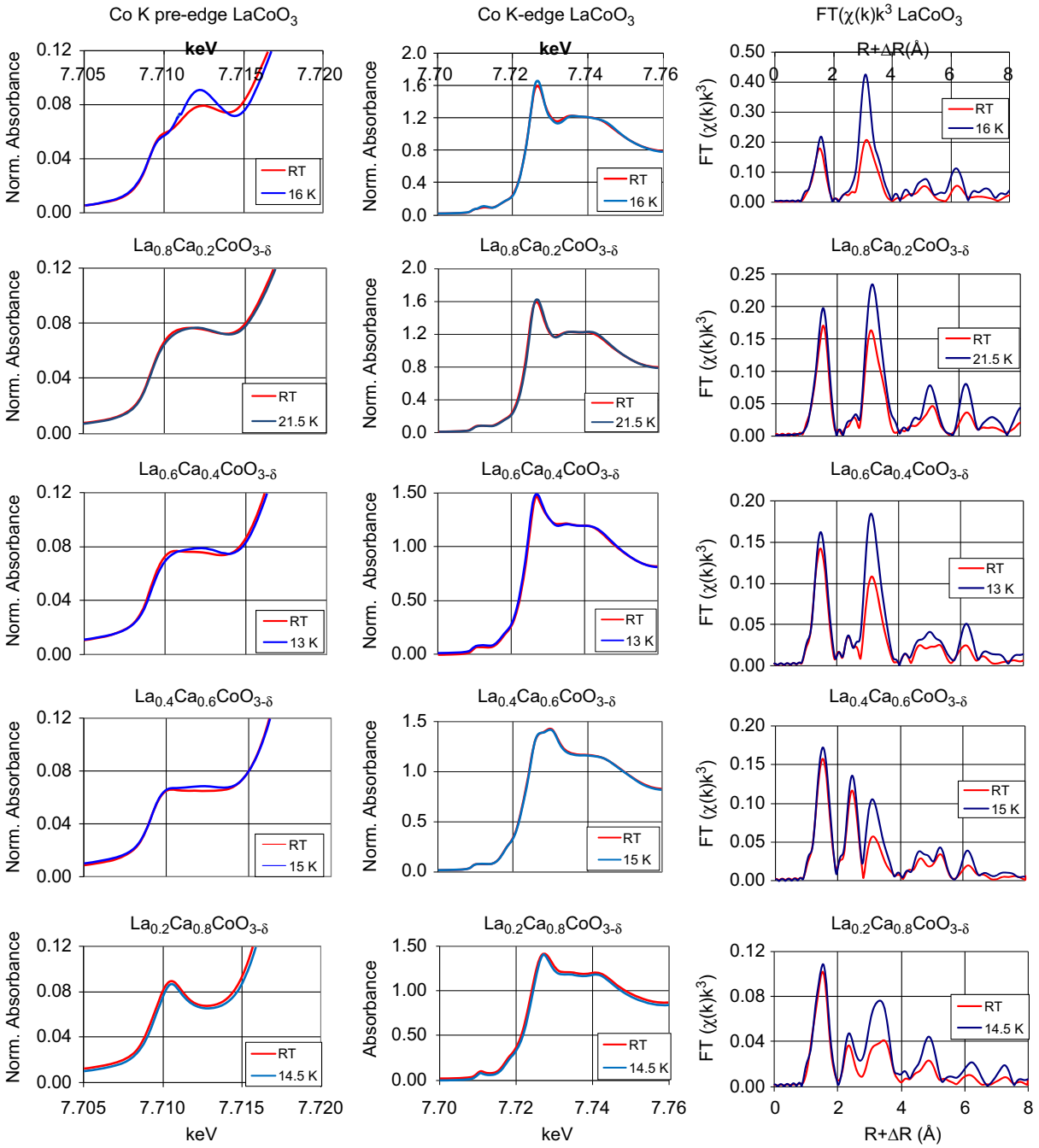

Fig. 1. >Comparison of low-temperature measurements with measurements at 300 K. First column: pre-edge regions of the investigated $La_{1-x}Ca_xCoO_{3-\delta}$ samples. Second column: XANES regions. Third column: Fourier transformed χ^*k^3 functions. In subsequent rows: Samples with x: 0, 0.2, 0.4, 0.6, 0.8, where the low-temperature spectra are as indicated presented in the same plots.

transitions may also have small dipolar contributions due to d–p hybridization of the cobalt or iron cation and metal–oxygen molecular orbitals Co(3d)–O(2p). A detailed discussion about dipole and quadrupole contributions to the pre-edge transitions of the Co K-edge in $LaCoO_3$ was published recently in connection with a low temperature X-ray absorption study in the partial fluorescence yield mode by Medarde et al. [21]. Our pre-edge features measured in the transmission mode are due to transitions to anti-bonding t_{2g}^* and e_g^* orbitals of cobalt and iron, respectively. They are not well separated with the exception of $LaCoO_3$, where a shoulder at 7710 eV and a peak at 7712.5 eV clearly indicate the expected crystal field splitting between the t_{2g} and e_g orbitals of about 2.3 eV. The fact that $LaCoO_3$ shows transitions to both t_{2g}^* and e_g^* bands is an indication for an intermediate or high spin state of Co(III) in this perovskite. For an undistorted cubic structure with six oxygen ligands, Co(III) is expected to be in the low spin ground state with a π^* (t_{2g}^6) configuration and 1A1 symmetry. Since all t_{2g} orbitals are occupied in this configuration only transitions to the σ^* (e_g) orbitals would be possible. In cobalt oxides Hund's interaction energy (energy difference between spin up and down) also called interatomic exchange energy is about half that of the ligand field splitting energy. For $LaCoO_3$ Hund's interaction energy is about 1–1.3 eV [15,22,40]. The splitting due to the intra-atomic Hund's exchange energy is not resolved in our pre-edge spectrum. At low-temperature these perovskites have the tendency to

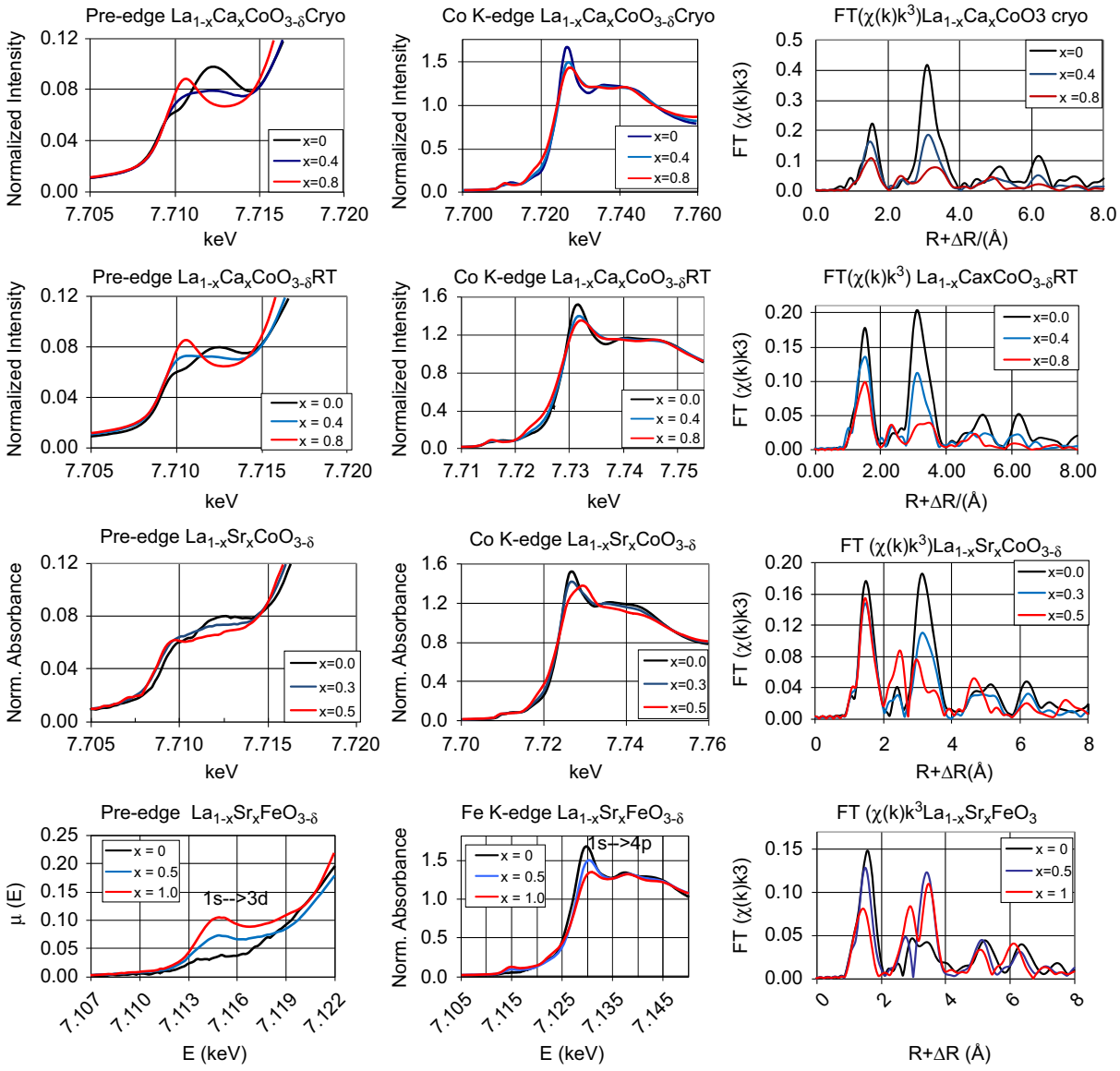

Fig. 2. x-dependency of the $La_{1-x}Ca_xCoO_{3-\delta}$, $La_{1-x}Sr_xCoO_{3-\delta}$ and $La_{1-x}Sr_xFeO_{3-\delta}$ series with three representative samples as indicated in the figures. First column: Pre-edge features. Second column: XANES region. Third column: FT $k^3\chi(k)$ function. First row: Low-temperature measurements of the $La_{1-x}Ca_xCoO_{3-\delta}$ series. Second row: 300 K measurements of the $La_{1-x}Ca_xCoO_{3-\delta}$ series. Third row: 300 K measurements of the $La_{1-x}Sr_xCoO_{3-\delta}$ series. Fourth row: 300 K measurements of the $La_{1-x}Sr_xFeO_{3-\delta}$ series.

switch to low spin states, which is very well demonstrated in Fig. 1 first row, where the *cold* $LaCoO_3$ sample has a much stronger pre-edge peak at 7712.5 eV indicating that the t_{2g}^* orbital's are almost filled and most of the transition goes to e_g^* orbitals. However, even at low temperature the spin state seems not to be 100% low spin, which was also found by Medarde et al. [21]. They called this spin state covalent intermediate state because of the presence of O 2p holes induced by a ligand to metal charge transfer.

An unambiguous interpretation of the x dependency of these pre-edge features is more difficult. First of all, there is only little difference in the pre-edge features between the samples at low temperature and at 300 K for the samples with $x > 0$ and for these perovskites a clean low spin state also seems not possible at low temperature. One potential reason for that is that the X-rays dissipate thermal energy in the sample and thus the actual sample temperature is higher than the reading of the thermo-couple at the sample holder. But since the beam intensity after the double mono-chromator is very low and the FT $k^3\chi(k)$ functions (third column in Fig. 1) are strongly increasing in intensity due to a lower Debye–Waller factors (expected at low temperatures) we think that the samples had the indicated low temperature.

The fact that the maximum in the pre-edge absorption is shifted to lower energy with increasing x especially in the $La_{1-x}Ca_xCoO_{3-\delta}$ samples is somehow striking. If substitution of La by Ca or Sr would increase the valence state we would expect that the low spin configuration would be favoured. This should lead to a similar intensity change in the pre-edge as with $LaCoO_3$ by decreasing the temperature (transitions to e_g^* becoming more important). In addition we would also expect that the total intensity of the pre-edge features would increase (increase in empty d-orbitals). None of these effects can be recognized in these Co perovskites. Contrarily, we find constant total pre-edge band intensities and even a weak decrease of the pre-edge bands with increasing x for the $La_{1-x}Sr_xCoO_{3-\delta}$ samples and especially for the $La_{1-x}Ca_xCoO_{3-\delta}$ samples a rather strong increase at the low energy side (presumable transitions to empty t_{2g}^*-orbitals)

together with a decrease of the pre-edge bands at the higher energy side. This is also an indication that the valence state of cobalt does not increase with increasing x, which is most likely due to the fact that the ligand to metal charge transfer (LMCT) process becomes more important with increasing x. This leads to ligand holes and oxygen vacancies with a somewhat lower crystal field splitting.

A quantitative discussion of the dependency of the pre-edge absorption on the substitution parameter x is challenging because we have to be aware of the fact that the $1s \rightarrow 3d$ multiplet transitions is complex since (1) the system is not strictly cubic, (2) the interatomic exchange energy is comparable to the crystal field energy and (3) the energy difference between the different spin states is very low thus the $3d$ metal cations in these perovskites contain probably a mixture of spin states with different energy levels.

In contrast to the Co perovskites the $La_{1-x}Sr_xFeO_{3-\delta}$ perovskites exhibit a clear increase of the pre-edge features upon increasing x. Thus with increasing x at least part of the Fe^{3+} d^5 is transformed to Fe^{4+} d^4, which offers additional transition possibilities to empty d-orbitals. However, for $x=1$ the total pre-edge intensity is increased by about 2.5 times compared to the sample with $x=0$. This can not only rationalized by additional empty d-orbitals. Obviously the dipolar transition probabilities are also increasing with x due to stronger d–p hybridization in the iron atoms and stronger Fe($3d$)–O($2p$) molecular orbitals overlap at higher valence states. In the investigated Co perovskites the valence state is not increasing with x thus the Co($3d$)–O($2p$) molecular orbitals overlap remains constant (total pre-edge intensity is not changing with x).

The shoulders at the foot of the K-edge at about 7716 eV for the Co perovskites and at about 7123 eV for the Fe perovskites are an additional pre-edge feature in the XANES region of these perovskites. In the $La_{1-x}Sr_xFeO_{3-\delta}$ series this feature is not increasing with x as much as for the Co perovskites. It has been assigned to an $1s \rightarrow 4p$ transition followed by a LMCT shake-down process. For Co(III) the shake-down process, which takes place after the primary $1s \rightarrow 4p$ excitation can be described as follows: $1s^1\underline{c}3d^64p^1 \rightarrow 1s^1\underline{c}3d^74p^1\underline{L}$ ($\underline{L}$=ligand hole, $\underline{c}$=core hole) [49,50], and for Fe(IV): $1s^1\underline{c}3d^44p^1 \rightarrow 1s^1\underline{c}3d^54p^1\underline{L}$.

3.3.2. K-edge energies

If the valence state is increasing we would expect a chemical shift of the K-edge (first derivative of the $1s \rightarrow 4p$ transition or of the half-height of the $1s \rightarrow 4p$ transition) to higher energies since at higher valence state, electrons are more strongly bound to the transition metal nucleus, which is especially the case for core electrons. But we observe virtually no K-edge energy shift as a function of x for the $La_{1-x}Ca_{0x}CoO_{3-\delta}$ and $La_{1-x}Sr_xCoO_{3-\delta}$ series. The $La_{0.2}Ca_{0.8}CoO_{3-\delta}$ sample has even a slightly lower K-edge energy (see numerical data in Tables 1 and 2 for the $La_{1-x}Ca_xCoO_{3-\delta}$ and $La_{1-x}Sr_xCoO_{3-\delta}$ series). The K-edge energy is slightly higher for the low temperature sample (0.1–0.3 eV).

However, the Fe K-edge of the $La_{1-x}Sr_xFeO_{3-\delta}$ perovskites is shifting to higher energies with increasing x. The edge at half-height is shifting by about 0.7 eV, and at the maximum of the white line by about 1 eV when going from $x=0$ to $x=1$. This shift is smaller than anticipated if the valence state is increased by one unit. The Fe K-edge would shift about 3.5–4 eV to higher energies when the valence state changes from Fe^{2+} to Fe^{3+} in iron oxides [51,52]. If Fe^{3+} is oxidized to Fe^{4+} the shift is smaller due to a lower relative charge change and probably also due to a more covalent nature of the Fe–O bond, which transfers some charge from oxygen to iron. This is compensating part of the positive charge on the iron nucleus. The Fe K-edge shift may also be lowered a bit due to a stronger LMCT shake-down band with increasing x, which creates a shoulder at the edge and shifts the visual edge to lower energies.

3.3.3. Maximum intensity at the absorption edge (white line)

With increasing x the white line is less pronounced. This is in line with the general observation that ionic compounds show strong and sharp white lines, whereas metals and compounds with covalent bonds show more diffuse white lines. This partial attenuation of the dipole allowed $1s \rightarrow 4p$ transition can be due to several reasons. It could be due to the partial substitution of La^{3+} by Ca^{2+} or Sr^{2+}, which leads to an energy dispersion due to transition metal atoms with unequal environment. In fact the Debye–Waller Factors listed in Tables 1–3 have the tendency to increase with increasing x *indicating additional disorder*. An explanation could also be a shortening of the lifetime of the excited state and of the $1s$ core hole of the Ca substituted compounds. A shorter lifetime of the excited state for $La_{0.5}Ca_{0.5}CoO_{3-\delta}$ is expected due to a lower symmetry in the partially Ca substituted compounds. The LMCT shake down process is also contributing to this effect it is enhanced in the Ca or Sr substituted perovskites (see discussion pre-edge features). The shake down process follows the initial $1s \rightarrow 4p$ excitation and takes intensity from this transition.

3.4. EXAFS investigation

The extended X-ray absorption fine structures (EXAFS) of the X-ray absorption spectrum and its FT $k^3\chi(k)$ functions (third column in Figs.1 and 2) contain valuable information about the nearest neighbors distances, the coordination number and coordination geometry. From the Co–O distances information about the cobalt valence state can be deduced. In theory, the oxygen coordination number obtained from EXAFS analysis would also lead to information about the valence state. But the coordination

Table 1
r_{Co-O} fits of the $La_{1-x}Ca_xCoO_{3-\delta}$ series measured at 300 K and at low-temperatures.

Perovskite	$(r1+r2)/2$	$r2-r1$	K-edge	r1				Residule1	r2		Residule2
	Å	Å	keV	Å	N	σ^2	$S0_2$	%	Å	σ^2	%
$LaCoO_3$ 16 K	1.9213	0.0029	7.7248	1.9199	5.54	0.0016	0.8308	3.45	1.9228	0.0028	5.59
$LaCoO_3$ 300 K	1.9225	0.0022	7.7245	1.9214	5.57	0.0029	0.8349	2.85	1.9236	0.0040	6.03
$La_{0.8}Ca_{0.2}CoO_{3-\delta}$ 21.5 K	1.9241	0.0020	7.7248	1.9231	5.65	0.0024	0.8475	3.99	1.9251	0.0033	5.26
$La_{0.8}Ca_{0.2}CoO_{3-\delta}$ 300 K	1.9252	0.0001	7.7246	1.9252	5.80	0.0028	0.8702	3.95	1.9253	0.0044	5.42
$La_{0.6}Ca_{0.4}CoO_{3-\delta}$ 13 K	1.9127	0.0029	7.7248	1.9113	5.41	0.0031	0.8120	8.11	1.9142	0.0048	9.62
$La_{0.6}Ca_{0.4}CoO_{3-\delta}$ 300 K	1.9120	0.0032	7.7245	1.9104	5.47	0.0041	0.8209	6.98	1.9136	0.0056	8.03
$La_{0.4}Ca_{0.6}CoO_{3-\delta}$ 15 K	1.9122	0.0040	7.7248	1.9102	5.38	0.0025	0.8062	6.69	1.9142	0.0041	8.47
$La_{0.4}Ca_{0.6}CoO_{3-\delta}$ 300 K	1.9110	0.0035	7.7246	1.9093	5.37	0.0032	0.8053	6.93	1.9128	0.0050	9.13
$La_{0.2}Ca_{0.8}CoO_{3-\delta}$ 14.5 K	1.9035	0.0047	7.7241	1.9011	4.73	0.0038	0.7098	5.46	1.9058	0.0082	17.00
$La_{0.2}Ca_{0.8}CoO_{3-\delta}$ 300 K	1.9049	0.0039	7.7240	1.9030	4.71	0.0045	0.7060	4.80	1.9069	0.0093	16.72

Table 2
r_{Co-O} fits of the $La_{1-x}Sr_xCoO_{3-\delta}$ series measured at 300 K.

Perovskite	$(r1+r2)/2$	$r2-r1$	K-edge	$r1$				Residule1	$r2$		Residule2
	Å	Å	keV	Å	N	σ^2	$S0_2$	%	Å	σ^2	%
$LaCoO_{3-\delta}$ 300 K	1.9230	0.0028	7.7245	1.9215	5.49	0.0025	0.8236	6.76	1.9244	0.0040	8.38
$La_{0.9}Sr_{0.1}CoO_{3-\delta}$ 300 K	1.9220	0.0010	7.7243	1.9215	5.73	0.0037	0.8565	13.08	1.9225	0.0045	12.95
$La_{0.8}Sr_{0.2}CoO_{3-\delta}$ 300 K	1.9235	0.0034	7.7245	1.9218	5.48	0.0030	0.8227	5.92	1.9252	0.0044	7.46
$La_{0.7}Sr_{0.3}CoO_{3-\delta}$ 300 K	1.9269	0.0024	7.7245	1.9257	5.66	0.0045	0.8489	12.22	1.9281	0.0056	11.95
$La_{0.6}Sr_{0.4}CoO_{3-\delta}$ 300 K	1.9280	0.0028	7.7245	1.9266	5.58	0.0040	0.8365	8.67	1.9294	0.0054	10.52
$La_{0.5}Sr_{0.5}CoO_{3-\delta}$ 300 K	1.9205	0.0045	7.7245	1.9183	5.46	0.0038	0.8191	10.89	1.9228	0.0054	11.22
$La_{0.5}Sr_{0.5}CoO_{3-\delta}$ 300 K	1.9209	0.0038	7.7245	1.9190	5.52	0.0042	0.8286	13.16	1.9228	0.0057	13.06

Table 3
r_{Fe-O} fits of the $La_{1-x}Sr_xFeO_{3-\delta}$ series measured at 300 K.

Perovskite	$(r1+r2)/2$	$r2-r1$	K-edge	$r1$				Residule1	$r2$		Residule2
	Å	Å	KeV	Å	N	σ^2	$S0_2$	%	Å	σ^2	%
$LaFeO_{3-\delta}$ 300 K	2.0017	0.0004	7.1280	2.0015	5.87	0.0041	0.8800	16.07	2.0019	0.0045	9.45
$La_{0.5}Sr_{0.5}FeO_{3-\delta}$ 300 K	1.9462	0.0008	7.1280	1.9458	5.10	0.0038	0.7651	10.99	1.9466	0.0069	14.00
$SrFeO_{3-\delta}$ 300 K	1.9021	−0.0030	7.1279	1.9036	5.18	0.0081	0.7773	4.27	1.9006	0.0113	7.71

number is strongly coupled with other EXAFS parameters especially with the Debye–Waller Factor and the amplitude reduction factor.

The FT $k^3\chi(k)$ functions shown in the third columns of Figs. 1 and 2 show dominant peaks at $R=1.5$ Å and at $R=3.1$ Å, where R stands for the phase and amplitude uncorrected radius in Ångstroms of the first and the second atomic shells around the X-ray absorbing transition metal (Co or Fe). The effective radii r_{eff} of the atomic shells are about 0.4–0.5 Å larger than the phase and amplitude uncorrected R-values obtained from the position of the peaks of FT of $k^3\chi(k)$ function. r_{eff} of the different shells can be obtained using phase and amplitude data from reference substances or from theoretical FEFF simulations. The first peaks of FT of $k^3\chi(k)$ function are due to the Me–O scattering paths, whereas the second dominant peak at about $R=3.1$ Å, and the intermediate peak at about $R=2.4$ Å contain scattering contributions of several scattering paths e.g. Co–La, Co–Ca, Co–Co, and several multi-scattering contributions like Co–O–O, Co–O–Co–O and so on. The peaks at higher k values are even more complicated rendering valuable interpretation and simulations of these scattering features questionable due to too many scattering paths, which contribute to these peaks. The first peak, however, contains structural information only from the Co–O scattering paths, and structural data are therefore very reliable especially if all six oxygen have the same distances to the transition metal.

We evaluated the Co–O and Fe–O distances using FEFF simulations, where we assumed octahedral coordination of the oxygen ligands with equal distances of all M–O bonds. $La_{1-x}Ca_xCoO_{3-\delta}$, $La_{1-x}Sr_xCoO_{3-\delta}$ and $La_{1-x}Sr_xFeO_{3-\delta}$ are anticipated to have either cubic symmetry ($Pm3m$, space group ITC no. 221) [42,48,53,54], rhombohedral symmetry ($R-3c$, space group no. 167) [27,42,48] or orthorhombic symmetry ($Pbnm$, space group ITC no. 62) [27,55] or even $I2/a$ space group symmetry (ITC no. 15) [22,43].

In the cubic and rhombohedral space groups the six oxygen ions are octahedrally coordinated with six equal transition metal oxygen distances, where in the space groups 62 and 15 three slightly different metal–oxide distances are expected. Assuming octahedral coordination for all investigated compounds is therefore strictly not correct. But the structures of the perovskites do not differ very much from an octahedral coordination with equal metal to oxygen distances and the resolution of the FT $k^3\chi(k)$ is not sufficient for unambiguous determination of three different metal to oxygen distances. It only allows the determination of an average value of these distances. Since some of the parameters are heavily correlated (especially N, σ^2 and S_0^2), we made a fit without fixing any parameter and a second fit where we fixed the coordination number (N) of oxygen to 6 and the amplitude reduction factor (S_0^2) to 0.9, an often recommended value. From a stoichiometric point of view N could vary between 6 and 5.5 in these series. As mentioned above the fitted N is rather meaningless. Fixing N to 6 and S_0^2 to 0.9 is closer to reality. If similar compounds have to be compared it is also advantageous to use the same amplitude reduction factor (S_0^2) for all of those compounds. The remaining flouting parameters are then r_{eff}, σ^2 and ΔE_0, where ΔE_0 (which is an E_0 correction) is expected to be close to zero and should not exceed 1–2 eV, which was the case for all simulations. The columns $r1$, N, σ^2,S_0^2 and Residule1 in Tables 1–3 list the data of the unrestricted fits and the later columns $r2$, σ^2, Residule2 list the data of the fits where we fixed the coordination number (N) to 6 and the amplitude reduction factor (S_0^2) to 0.9. The K-edge energy (keV) was obtained from the maximum of the first derivative at the K-edge. The column $(r1+r2)/2$ indicates the average r_{eff} values obtained from both fits. $r2-r1$ indicates the r_{eff} values differences between the two fits. The differences between the r_{eff} values are very small. The maximum deviation of the two fits is only 5 hundreds of an Ångstrom. The Residule1 and Residule2 give an idea of the goodness of the fits. As expected the fits with unrestricted parameters give lower Residules.

Due to a lower Debye–Waller factor (σ^2) at low temperatures (lower dynamic uncertainties) the FT $k^3\chi(k)$ signals (see Fig. 1 third column) are much stronger for the samples measured at low temperatures. Table 1 shows that in fact σ^2 is considerably lower for the low temperature measurements. The effect is so strong and systematic that it could probably even be used for an indirect temperature determination. At least it is a reliable indication that our samples are not heated by the incident X-rays of the XAS investigation.

The intensities of the first and the second peaks of the FT $k^3\chi(k)$ functions caused by the Me–O scattering paths are decreasing with x (see Fig. 2 third column). For the $La_{1-x}Ca_xCoO_{3-\delta}$ and the $La_{1-x}Sr_xFeO_{3-\delta}$ series the intensities of these peaks are decreasing with x down to about half the intensity of the unsubstituted perovskites. For the $La_{1-x}Sr_xCoO_{3-\delta}$ series the range of x was

smaller, which explains the smaller decrease of the FT $k^3\chi(k)$ function in this series. Introducing Ca or Sr causes a static disorder in the perovskite and an increase of the Debye–Waller Factor (σ^2). The intensity of the FT $k^3\chi(k)$ function is almost inversely proportional to the Debye–Waller Factor. Especially in the case of the $La_{1-x}Sr_xFeO_{3-\delta}$ series the formation of the Jahn–Teller ion Fe^{4+} (h.s. d^4) is also leading to a dynamic distortion of the Fe–O_6 octahedron and thus to a higher Debye–Waller Factor.

Oxygen vacancies would decrease the number of scattering paths due to lower coordination numbers and could therefore also contribute to the intensity decrease of the FT $k^3\chi(k)$ function but, its influence would be lower. The increase of the Debye–Waller Factor (σ^2) with x is confirmed by the data listed in Tables 1–3.

The decrease in intensity in the second shell (second peak of the FT $k^3\chi(k)$ functions) is in addition due to the weaker scattering properties of Ca^{2+} or Sr^{2+} compared to La^{3+}.

Here we make no effort for a quantitative evaluation of the second shell since too many parameters would have to be fitted and it would not contribute much to our main goal of the determination of the valence states of cobalt and iron.

Examining the FT $k^3\chi(k)$ signals (see Figs. 1 and 2 third column) of $La_{0.4}Ca_{0.6}CoO_{3-\delta}$ and $La_{0.5}Sr_{0.5}CoO_{3-\delta}$ we think that these two samples contain two phases. The FT $k^3\chi(k)$ signals of these two samples have prominent peaks at position typical for Co_3O_4 (A reference spectrum of Co_3O_4 was published e.g. by Hueso et al. [33].) The interpretation of the XAS spectra of these two samples may be questionable since they do not correspond to clean perovskite structured $La_{0.4}Ca_{0.6}CoO_{3-\delta}$ and $La_{0.5}Sr_{0.5}CoO_{3-\delta}$ samples.

The most reliable parameter of the EXAFS fitting results is the metal to oxygen distance (r_{eff}). It is also the best indicator for the cobalt and iron valence states of the investigated samples. Since the r_{eff} values of the $La_{1-x}Ca_xCoO_{3-\delta}$ and $La_{1-x}Sr_xCoO_{3-\delta}$ series are very close to the r_{eff} value of $LaCoO_3$ (the r_{eff} decrease for the highest x value is only about 0.02 Å). We conclude that the valence state for cobalt of the entire series is very close to Co^{3+}. We made also a fit for $La_{0.5}Ca_{0.5}CoO_{2.75}$, with a fixed coordination number $N=5.5$, which led to a slightly better fit with a somewhat smaller Debye–Waller Factor than the fit of $La_{0.5}Ca_{0.5}CoO_3$ with $N=6$. This is also an indication that $La_{0.5}Ca_{0.5}CoO_{2.75}$ (Co^{3+}) is the more accurate formula.

The ionic radii of Co^{3+} and therefore also the Co–O distance depend on the spin state. High spin states of Co and Fe have more electrons in antibonding e_g^* orbitals thus low spin configurations lead to slightly lower ionic radii [56]. The results of the least square fits of the Co–O and Fe–O distances are summarized in Tables 1–3.

An estimation of the error bars in Tables 1–3 leads to an error of about ± 0.005 Å for the metal oxygen distances.

For the Co–O distance the difference between the low temperature sample and the sample at room temperature is not so clear. At least at low x values the low temperature sample has a slightly lower Co–O distance. Since the valence state of cobalt is not increasing with x in the cobalt perovskites, oxygen vacancies or partial oxidation of the oxygen ligands (ligand holes) have to compensate for the charge deficit introduced by substituting La^{3+} with Ca^{2+} or Sr^{2+} in these perovskites.

The r_{eff} of the Fe–O bond is varying much more in the $La_{1-x}Sr_xFeO_{3-\delta}$ series. It shifts by 0.1 Å over the x-range measured, which clearly indicates an increase of the valence state of iron with x. Typically the Fe–O distance is in the range of 1.91–1.95 Å for Fe(IV), and 1.990–2.006 Å for Fe(III), whereas the distance in Fe(II) oxides is about 2.14 Å. Our r_{eff} values of the Fe–O bond correspond well to Fe(III) for $LaFeO_3$ and to Fe(IV) for $SrFeO_3$.

3.5. Iodometric titration

The spectroscopic result that the valence states of the cobalt perovskites do not increase with x has been independently confirmed with iodometric titrations. This method is very accurate but not unproblematic to perform. The Co perovskites have to be dissolved in strong acids under rigorous oxygen exclusion in presence of an excess of potassium iodide (KI), which is oxidized to I_2 by Co(III) and Co(IV). At these conditions there is a chance that some of the iodine escapes in the gas phase especially if the solution is bubbled with argon or nitrogen during dissolution. We therefore developed a method where the iodine is titrated while the perovskite is dissolved. The procedure and the used apparatus were described in a former publication [37]. Since these perovskites have the tendency to absorb CO_2 and H_2O if stored in air we determined this additional weight using thermogravimetry to make corrections of the initial weight. The iodometric titration was performed with $LaCoO_3$ and $La_{0.5}Ca_{0.5}CoO_{3-\delta}$ samples. The results of this investigation are listed in Table 4. It clearly indicates a valence state of 3^+ for these samples, which is in perfect agreement with the spectroscopic data.

Table 4
Iodometric titration of $LaCoO_3$ and $La_{0.5}Ca_{0.5}CoO_{3-\delta}$. The adsorbed mg CO_2 and H_2O were evaluated using thermogravimetry described in [35].

Sample	MW (g)	Sample weight (mg)	Adsorbed CO_2 and H_2O (mg*)	0.05 M $Na_2S_2O_3$ (ml)	Valence state
$LaCoO_3$	245.85	11.37	0.19	0.908	2.99
$LaCoO_3$	245.85	11.81	0.19	0.959	3.04
$LaCoO_3$	245.85	12.06	0.19	0.969	3.01
$La_{0.5}Ca_{0.5}CoO_{0.75}$	192.43	30.38	0.61	3.130	3.04
$La_{0.5}Ca_{0.5}CoO_{0.75}$	192.43	32.22	0.64	3.282	2.99

From the results of the iodometric titration we may also conclude that oxygen vacancies are compensating the missing charge introduced if La^{3+} is replaced by Ca^{2+} or Sr^{2+}. If ligand holes (O^{-1} or O_6^{-11}) would compensate the charge, these holes would most probably have the potential to oxidize iodide ions to iodine as much as Co(III) does. In the $La_{1-x}Sr_xFeO_{3-\delta}$ series the situation is different. The charge compensation is achieved by a valence state increase of iron and if LMCT takes place, expected due to the higher charge at the iron, it does not end up with oxygen vacancies due to a strong covalent Fe–O bond.

4. Conclusions

The K-edge X-ray absorption spectroscopy is a valuable tool to evaluate the valence state and the electronic structure of transition metals in perovskites. Especially the r_{eff} values of the M–O distances as determined by EXAFS offer reliable information about the valence state. In addition the pre-edge bands and the K-edge position are sensitive to the valence state whereas the electronic structure can be read from the pre-edge features.

The Co K-edge energy, Co–O distances and the total pre-edge intensity remain almost constant in our $La_{1-x}Ca_xCoO_3$ and $La_{1-x}Sr_xCoO_3$ series independent of x and temperature. This allows the conclusion that the cobalt remains close to the valence state of 3^+ in these series thus δ should be very close to $x/2$. From the intensity change in the pre-edge bands we conclude an increase in t_{2g}^* and a decrease in e_e^* orbital occupancy going to low temperatures. Increasing x we have the inverse intensity change in the Co K pre-edge features presumably indicating a decrease of t_{2g}^* occupancy. This is pointing to LMCT with creation of ligand holes and ligand vacancies (oxygen vacancies), which leads to a lower crystal field energy and probably to a high spin configuration with more empty t_{2g}^* orbitals. But, the situation is rather complex due to the fact that the energy levels of the compounds with ligand holes or ligand vacancies may shift.

This makes the interpretation questionable as long as we have no proof that the low energy pre-edge band is really a $1s \rightarrow t_{2g}^{*}$ transition.

The situation is different for the $La_{1-x}Sr_xFeO_{3-\delta}$ series, where the intensity of the pre-edge features is strongly increasing with x, the r_{Fe-O} values are decreasing with x and the Fe K-edge of the $La_{1-x}Sr_xFeO_{3-\delta}$ perovskites is shifting to higher energies. These are strong arguments for a valence state, which is increasing with x. The data indicate that the valence state of the $La_{1-x}Sr_xFeO_{3-\delta}$ perovskites increases as much as x is increasing thus δ should be very close to 0.

Apparently for cobalt perovskites the charge compensation takes place via oxygen vacancies whereas for the iron perovskites the charge compensation is achieved by an increase of the iron valence state, which generates a more covalent Fe–O bond, with some charge transfer from oxygen to iron. However, the strong covalent nature of the Fe–O bond does not allow oxygen vacancies.

Acknowledgments

We like to acknowledge A. Schuler of the Paul Scherrer Institute for the excellent experimental support concerning the iodometric titration. Portions of this research were carried out at the Stanford Synchrotron Radiation Lightsource, a national user facility operated by Stanford University on behalf of the U.S. Department of Energy, Office of Basic Energy Sciences. A. Braun is grateful for financial support by the European Commission within the projects MIRG HiTempEchem # CT-2006-042095 and Real-SOFC # SES6-CT-2003-502612. Part of this research was carried out at the Stanford Synchrotron Radiation Lightsource, a national user facility operated by Stanford University on behalf of the U.S. Department of Energy, Office of Basic Energy Sciences.

Appendix A. Supplementary materials

Supplementary data associated with this article can be found in the online version at doi:10.1016/j.jssc.2011.09.027.

References

[1] (b) R.J.H. Voorhoeve, Advanced Materials in Catalysis, Academic Press New York, 1977;
(b) W.F. Libby, Science 171 (1971).
[2] S. Müller, K.A. Striebel, O. Haas, Electrochim. Acta 39 (1994) 1661.
[3] M. Bursell, M. Pirjamali, Y. Kiros, Electrochim. Acta 47 (2002) 1651.
[4] R.N. Singh, S.P. Singh, N.K. Singh, S.K. Tiwari, G. Poillerat, P. Chartier, J. Chem. Soc. Faraday Trans. 92 (1996) 2593–2598.
[5] S.P. Simmer, J.P. Shelton, M.,,D. Anderson, J.W. Stevenson, Solid State Ionics 161 (2003) 11–18.
[6] L.J. Gauckler, D. Beckel, B.E. Buergler, E. Jud, U.P. Muecke, M. Prestat, J.L.M. Rupp, J.R. Richter, Chimia 58 (2004) 837–850.
[7] U.F. Vogt, J. Sfeir, J. Richter, C. Soltmann, P. Holtappels, Pure Appl. Chem. 80 (2008) 2543–2552.
[8] P. Holtappels, U. Vogt, T. Graule, Adv. Eng. Mater. 7 (5) (2005) 1–11.
[9] R. Robert, S. Romer, A. Reller, A. Weidenkaff, Adv. Eng. Mater. 7 (2005) 303.
[10] B. Raveau, A. Maignan, Europhys. News 34 (6) (2003) 238.
[11] P.M. Raccah, J.B. Goodenough, Phys. Rev. 155 (1967) 932.
[12] M.A. Senaris-Rodriguez, J.B. Goodenough, J. Solid State Chem. 116 (1995) 224.
[13] P. Adler, A. Lebon, V. Damljanovic, C. Ulrich, C. Bernhard, A.V. Boris, A. Maljuk, C.T. Lin, B. Keimer, Phys. Rev. B 73 (2006) 094451.
[14] A. Braun, S. Shrout, A.C. Fowlks, B.A. Osaisai, S. Seifert, E. Granlund, E.J. Cairns, J. Synchrotron Radiat. 10 (2003) 320–325.
[15] V. Pralong, V. Caignaert, S. Hébert, C. Marinescu, B. Raveau, A. Maignan, Solid State Ionics 177 (2006) 815–820.
[16] T. Nakamura, G. Petzow, L.J. Gauckler, Mater. Res. Bull. 14 (1979) 649–695.
[17] B.G. Tilset, H. Fjellvag, A. Kjekshus, J. Solid State Chem. 119 (1995) 271.
[18] O. Toulemonde, N. N'Guyen, F. Studer, A. Traverse, J. Solid State Chem. 158 (2001) 208–217.
[19] O. Haas, F. Holzer, S. Müller, J.M. McBreen, X.Q. Yang, X. Sun, M. Balasubramanian, Electrochim. Acta 47 (2002) 3211.
[20] G. Vankó, J.-P. Rueff, A. Mattila, Z. Németh, A. Shukla, Phys. Rev. B 73 (2006) 024424.
[21] M. Medarde, C. Dallera, M. Grioni, J. Voigt, A. Podlesnyak, E. Pomjakushina, K. Conder, Th. Neisius, O. Tjernberg, S.N. Barilo, Phys. Rev. B 73 (2006) 054424.
[22] O. Haas, R.P.W.J. Struis, J.M. McBreen, J. Solid State Chem. 177 (2004) 1000–1010.
[23] G. Thronton, I.W. Owen, G.P. Diakun, J. Phys.: Condens. Matter 3 (1991) 417.
[24] M. Sahnoun, C. Daul, O. Haas, J. Appl. Phys. 101 (2007) 014911.
[25] Y. Jiang, F. Bridges, N. Sundaram, D.P. Belanger, I.E. Anderson, J.F. Mitchell, H. Zheng, Phys. Rev. B 80 (2009) 144423.
[26] O. Haas, U.F. Vogt, C. Soltmann, A. Braun, W.-S. Yoon, X.Q. Yang, T. Graule, Mater. Res. Bull. 44 (2009) 1397–1404.
[27] C.L. Chang, G. Chern, M.F. Tai, Y.W. Su, C.L. Dong, S.Y. Liu, C.S. Hwang, P.K. Tseng, Jpn. J. Appl. Phys. Suppl. 38 (1999) 108–110.
[28] J. Blasco, B. Aznar, J. Garcia, G. Subias, J. Herrero-Martin, J. Stankiewicz, Phys. Rev. B 77 (2008) 054107.
[29] A. Braun, J. Richter, A.S. Harvey, S. Erat, A. Infortuna, A. Frei, E. Pomjakushina, Bongjin S. Mun, P. Holtappels, U. Vogt, K. Conder, L.J. Gauckler, T. Graule, Appl. Phys. Lett. 93 (2008) 262103.
[30] S.C. Grice, W.R. Flavell, A.G. Thomas, S. Warren, P.G.D. Marr, D.E. Jewitt, N. Khan, P.M. Dunwoody, S.A. Jones, Int. J. Mol. Sci. 2 (2001) 197–210.
[31] V. Efimov, E. Efimova, D. Karpinsky, D.I. Kochubey, V. Kriventsov, A. Kuzmin, S. Molodtsov, V. Sikolenko, S. Tiutiunnikov, I.O. Troyanchuk, A.N. Shmakov, D. Vyalikh, Phys. Stat. Sol. (c) 4 (2007) 805–808.
[32] Y. Jiang, F. Bridges, N. Sundaram, D.P. Belanger, I.E. Anderson, J.F. Mitchell, H. Zheng, Phys. Rev. B 80 (2009) 144423.
[33] J.L. Hueso, J.P. Holgado, R. Pereniguez, S. Mun, M. Salmeron, A. Caballero, J. Solid State Chem. 183 (2010) 27.
[34] A. Piovano, G. Augustini, A.I. Frenkel, T. Bertier, C. Prestipino, M. Ceretti, W. Paulus, C. Lamberti, J. Phys. Chem. C 115 (2011) 1311.
[35] J.E. Sunstrom, K.V. Ramanujachary, M. Greenblatt, M. Croft, J. Solid State Chem. 139 (1998) 388.
[36] S.K. Tiwari, P. Chartier, R.N. Singh, J. Electrochem. Soc. 142 (1995) 148–153.
[37] O. Haas, Chr. Ludwig, A. Wokaun, Anal. Chem. 78 (2006) 7273–7277.
[38] ⟨http://www.cxro.lbl.gov⟩.
[39] T. Ressler, J. Synchrotron Radiat. 5 (1998) 118.
[40] A.L. Ankudinov, C.E. Bouldin, J.J. Rehr, J. Sims, H. Hung, Phys. Rev. B 65 (2002) 104107.
[41] Wold, R. Ward, J. Am. Chem. Soc. 76 (1954) 1029.
[42] G. Thornton, B.C. Tofield, A.W. Hewat, J. Solid State Chem. 61 (1986) 301.
[43] G. Maris, Y. Ren, V. Volotchaev, C. Zobel, T. Lorenz, T.T.M. Palstra, Phys. Rev. B 67 (2003) 224423.
[44] JCPDS-ICDD Database, Card No. 25-1060, 1998.
[45] JCPDS-ICDD Database, Card No. 48-0123, 1998.
[46] A. Wold, B. Post, E. Banks, J. Am. Chem. Soc. 79 (1957) 6365.
[47] N.M.L.P. Closset, R.H.E. van Doorn, H. Kruidhof, J. Boeijsma, Powder Diffr. 11 (1996) 3.
[48] S.E. Dann, D.B. Currie, M.T. Weller, M.F. Thomas, A.D. Al-Rawwas, J. Solid State Chem. 109 (1994) 134–144.
[49] M.G. Kim, Y.S. Im, E.J. Oh, K.H. Kim, C.H. Yo, Physica B 229 (1997) 338–346.
[50] A. Chainani, M. Mathew, D.D. Sarma, Phys. Rev. B 46 (1992) 9976–9983.
[51] M. Wilke, F. Farges, P.-E. Petit, G.E. Brown Jr., F. Martin, Am. Mineral. 86 (2001) 714–730.
[52] O. Haas, A. Deb, E.J. Cairns, A. Wokaun, J. Electrochem. Soc. 152 (2005) 1–6.
[53] M.K. Lal, M. Raghunandan, Gupta, R.N. Singh, Int. J. Hydrogen Energy 30 (2005) 723–729.
[54] R.H.E. van Doorn, A.J. Burggraaf, Solid State Ionics 128 (2000) 65–78.
[55] J.C. Burley, J.F. Mitchell, S. Short, J. C. Phys. Rev. B 69 (2004) 054401.
[56] C. Zobel, M. Kriener, D. Bruns, J. Baier, M. Grüninger, T. Lorenz, P. Reutler, A. Revcolevschi, Phys. Rev. B 66 (2002) 020402(R).